

# Where are the absorbers towards Q2302+029?

David V. Bowen<sup>1,2,3</sup>, Raul Jimenez<sup>4,5</sup>, Edward B. Jenkins<sup>1</sup> and Max Pettini<sup>6</sup>

<sup>1</sup> *Princeton University Observatory, Princeton, NJ 08544*

<sup>2</sup> *Royal Observatory, Blackford Hill, Edinburgh EH9 3HJ, UK*

<sup>3</sup> *Department of Physics & Astronomy, Johns Hopkins University, Baltimore, MD 21218*

<sup>4</sup> *Institute for Astronomy, University of Edinburgh, Blackford Hill, Edinburgh EH9 3HJ, UK*

<sup>5</sup> *Current address: Rutgers University, Dept. of Phys. & Astron., 136 Frelinghuysen Rd., Piscataway, NJ 08854*

<sup>6</sup> *Institute of Astronomy, Madingley Rd., Cambridge CB3 0HA, UK*

## ABSTRACT

We present images and spectroscopy of objects close to the sightline of Q2302+029 in order to search for galaxies responsible for the remarkable  $z = 0.7$  high-ionization absorption line system found by Jannuzi et al. (1996). This system shows ‘normal’ narrow O VI, N V, and C IV lines superimposed on broader (3,000–5,000 km s<sup>-1</sup> wide), unsaturated absorption troughs some 56,000 km s<sup>-1</sup> away from the QSO emission redshift ( $z_{\text{em}} = 1.052$ ). Despite reaching sensitivities sufficient to detect 1/10L\* galaxies in the optical and 1/20L\* in the infra-red, we are unable to detect any obvious bright galaxies which might be responsible for the absorption beyond  $\approx 6 h^{-1}$  kpc of the sightline. This supports the hypotheses that the absorption is either intrinsic to the QSO, or arises in intracluster gas. Adopting either explanation is problematic: in the first case, ‘associated’ absorption at such high ejection velocities is hard to understand, and challenges the conventional discrimination between intrinsic and intervening absorbers; in the second case, the gas must reside in a  $\sim 40 h^{-1}$  Mpc long filament aligned along the line of sight in order to reproduce the broad absorption. Since the absorption system is unusual, such a chance alignment might not be unreasonable.

Spectroscopy of objects beyond the immediate vicinity of the QSO sightline reveals a galaxy cluster at  $z = 0.59$ , which coincides with strong Ly $\alpha$  and more narrow high ionization lines in the quasar spectrum. Here too, the lack of galaxies at distances comparable to those found for, e.g., Ly $\alpha$ -absorbing galaxies, suggests that the absorption may arise from intracluster gas unassociated with any individual galaxies.

*Subject headings:* quasars:absorption lines—quasars:individual (Q2302+029)—large-scale structure of universe

## 1. Introduction

The transition of the O VI  $\lambda\lambda 1032, 1037$  absorption doublet seen in the spectra of QSOs has long been of interest because of the difficulty in producing O VI ions by photoionization alone. The ionization of O V to O VI requires photons with energies above 114 eV, which are rare except in the radiation field of QSOs and AGN. Traditionally, it has been thought that O VI absorption probably marks the existence of collisionally ionized gas, since under equilibrium conditions the fraction of oxygen residing as O VI in a plasma peaks at a temperature of  $T \sim 3 \times 10^5$  K (Sutherland & Dopita 1993). More recently, with the explosive devel-

opment of hydrodynamical simulations which follow the physical conditions of gas as galactic large-scale structure forms, it appears that a substantial fraction of baryons may be in a shock heated phase at temperatures of  $10^5 - 10^7$  K as a result of gravitational collapse (see, in particular, Cen & Ostriker 1999, and refs. therein). O VI absorption lines have been hard to detect at high redshifts due to confusion with the Ly $\alpha$ -forest (Lu & Savage 1993) but access to ultraviolet wavelength regions with the *Hubble Space Telescope* (HST) has made it possible to detect such systems at redshifts  $z < 1$  as the forest thins out (Burles & Tytler 1996; Bergeron et al. 1994; Jannuzi et al. 1998).

Moreover, recent work suggests that O VI systems are remarkably common at low redshift, and that the lower limit to the cosmological mass density contributed by such systems today may be comparable to, or exceed, that of stars and cool gas in galaxies, as well as X-ray emitting gas in galaxy clusters (Tripp et al. 2000; Tripp & Savage 2000).

In trying to understand the origin of the many types of QSO absorption line systems, the most obvious question to ask is whether the absorption is directly associated with galaxies. To date, the answer to this question has been surprisingly ambiguous for a wide range of absorber types. Despite initial detections of Mg II absorbing galaxies which seemed to firmly establish the existence of  $\sim 40 h^{-1} \text{ kpc}^1$  radii halos for bright galaxies (Bergeron 1986; Bergeron & Boisse 1991; Steidel et al. 1994), it remains unclear whether individual galaxies are responsible for Ly $\alpha$  lines (Lanzetta et al. 1995; Chen et al. 1998; Morris et al. 1993; Stocke et al. 1995; Bowen et al. 1996; Le Brun et al. 1996; Shull et al. 1996; van Gorkom et al. 1996; Bowen et al. 1998; Tripp et al. 1998), while the diversity of galaxy types associated with damped Ly $\alpha$  systems has been a surprise (Le Brun et al. 1997; Lanzetta et al. 1997; Rao & Turnshek 1998). Establishing whether O VI absorption is linked to galaxies is important for establishing whether absorption is indeed due to violent processes within the ISM of individual galaxies or the consequence of the growth of large-scale structure in the universe. The effort to understand these systems is now even more timely with the launch of the *Far Ultraviolet Spectroscopic Explorer* (FUSE) which will characterize the distribution of O VI absorbing gas in the Milky Way disk and halo, and in the Magellanic Clouds, since the data obtained will provide an important baseline for understanding the higher redshift systems.

For these reasons, we have begun a survey to search for the absorbers responsible for  $z < 1$  O VI absorption systems. Our approach is similar to those of previous studies — deep imaging of the field around the QSO followed by spectroscopic confirmation of detected objects. However, many of the O VI systems detected by *HST* are at redshifts almost inaccessible to spectroscopic observations with 4 m class telescopes. We have therefore aimed to obtain multicolor information — in particular, deep infra-red (IR) images — in

order to estimate galaxy redshifts photometrically. For example, in Figure 1 we show the spectral energy distribution (SED) of a late-type galaxy at  $z = 0.7$ . (We discuss these models in more detail in §3.3). The figure shows that the peak of a galaxy’s SED at these redshifts occurs at wavelengths between the optical and the IR; combining photometry in these two regimes should enable us to constrain a galaxy’s redshift.

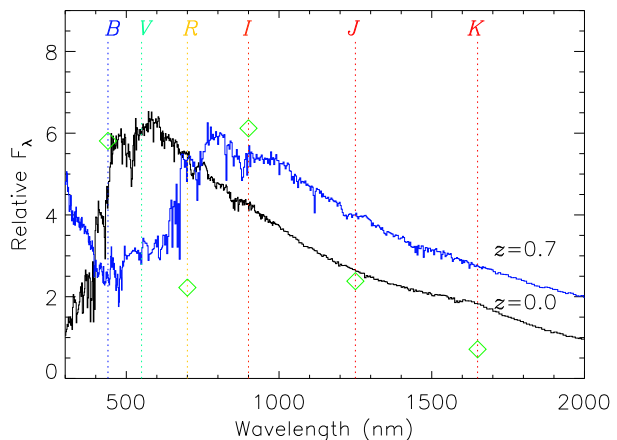


Fig. 1.— The dark curve shows the SED of a 10 Gyr old—i.e. present day—galaxy with metallicity of  $Z = 0.2 Z_{\odot}$  at  $z = 0$ . The lighter curve shows the same galaxy, when only 5 Gyr old at  $z = 0.7$ . The absolute normalization of the SEDs are arbitrary. The peak of the redshifted galaxy has shifted from between the B- and V-bands to between the R- and I-bands; with both optical and IR magnitudes measured for such a galaxy, it is possible to constrain the wavelength of the SED peak, and hence the object’s redshift. The diamonds denote the *relative* flux limits of our data towards Q2302+029. They are scaled such that  $F_{\lambda}(I)$  lies at the peak of the galaxy’s SED, and are discussed in the text.

In this paper we discuss some initial results of our survey, a search for galaxies towards the radio-quiet QSO Q2302+029 ( $z_{\text{em}} = 1.052$ ). *HST* spectra obtained by Jannuzi et al. (1996) show remarkable broad (FWHM  $\sim 3,000\text{--}5,000 \text{ km s}^{-1}$ ) O VI, N V, and C IV absorption at  $z = 0.695$ , with more typical narrow-lines (including Ly $\alpha$ , which is not seen as a broad component) superposed at  $z = 0.7106$ . Further, the system shows no low-ionization species such as Si II and Mg II. Jannuzi et al. considered three possible causes

<sup>1</sup>  $h = H_0/100$ , where  $H_0$  is the Hubble constant, and  $q_0 = 0.5$  is assumed throughout this paper

for the absorption: gas ejected by the QSO at a velocity of  $\sim 56,000 \text{ km s}^{-1}$ ; gas from galaxies and/or the intracluster medium of a cluster or supercluster; or gas from a supernova remnant in a single galaxy at a redshift similar to that of the narrow line system. Januzzi et al. were unable to distinguish between these three possibilities with the available data; clearly, a search for absorbing galaxies close to the line of sight is an important first step in attempting to unravel the origins of this unique system.

## 2. Observations and Catalogs

### 2.1. Imaging observations

*J*- and *K*-band images of the field around Q2302+029 were taken 1998-Sept-11 & 12 at the 3.8 m United Kingdom Infrared Telescope (UKIRT) on Hawaii using the IRCAM3 camera. The detector was a 256x256 Indium Antimonide (InSb) array, each pixel 0.286 arcsec square, giving a field of view of 73x73 arcsecs. Data were taken in NDSTARE mode, such that a single dark exposure was followed by nine minute exposures broken into nine 20x3 sec exposures in *J* and nine 10x6 sec exposures in *K*. (The pixels of the InSb array are quickly filled by photons because of the high sky background, so frequent read-out of the array is required.) After each one-minute exposure, the telescope was shifted by 8 arcsec, forming a grid of nine pointings in one nine-minute group, to enable production of an accurate flat-field (FF) during the reduction of the data. When the nine-minute group observation was completed, the center of the grid was shifted by 2 arcsec, and the nine-minute pattern repeated. Total exposure times of 72 and 170 mins were obtained for the *J*- and *K*-band images respectively. Observations of ‘faint’ UKIRT standard stars were also taken shortly before those of the QSO field.

To reduce the data, we used IRAF<sup>2</sup> to first subtract the dark frame from each of the nine-minute sub-exposures. Because the sky varies over short time intervals, the FF used to flatten the sub-exposures of a nine-minute pointing needed to be constructed from only the one-minute exposures comprising the group. Although the median of nine frames with high background counts produces an adequate signal-to-noise, the small number used means that ‘residuals’ in the

FF occur at the positions of the brightest objects in the frame. To overcome this, we defined circular masks at the positions of all bright objects in the (initial) flat-fielded image, using the *ximages* package of the IRAF PROs package. A new, more accurate, FF was constructed by forming the median of the nine individual frames, but with pixels in the masked regions excluded. Each sub-exposure was then shifted to a common reference position and a final coadded image produced. A small non-linearity correction was made, and a photometric zero-point calculated using the standard stars.

Harris *B*-, *R*-, and *I*-band images were taken with the Wide Field Camera (WFC) at the 2.5 m Isaac Newton Telescope on La Palma on 1998-Nov-22. The detector consists of four thinned EEV 2Kx4K CCDs each with a plate scale of 0.33 arcsec pixel<sup>-1</sup> and a coverage of 22.8x11.4 arcmin. Exposures of 400 sec were taken at pointings differing by ten arcsecs. Total exposure times of 53.3, 26.7 and 20.0 mins were obtained for the *B*, *R*, and *I*-bands respectively, and the data were bias-subtracted and flat-fielded with dome flats in the standard manner. The *I*-band data suffered from severe fringing; to remove this, the flat-fielded *I* frames were medianed to produce a fringe frame with a mean of zero which was scaled to, then subtracted from, each *I*-band frame. Photometric zero points were derived from standard star exposures bracketing the science data, and a correction was applied for non-linearities in the electronics.

### 2.2. Photometric catalogs and magnitude limits

To detect and catalog galaxies in our images, we ran the *sExtractor* routines (Bertin & Arnouts 1996) on each of the five science frames. Catalogs of objects from each passband were merged, and appropriate extinction corrections were applied to the derived magnitudes.

In Table 1 we list all the objects detected within a radius of 0.67 arcmins; this corresponds to  $160 h^{-1} \text{ kpc}$  at  $z = 0.7$ , which is the radius found by Lanzetta et al. (1995) for Ly $\alpha$ -absorbing halos, and which we therefore consider to be the radius of interest. In principle, O VI absorbing halos might be larger than this, but the examination of the objects closest to the line of sight naturally received the highest attention. Objects without *J* and *K* entries in Table 1 were not within the IRCAM field of view.

The magnitude limits for each passband are given

<sup>2</sup>The Image Reduction and Analysis Facility (IRAF) software is provided by the National Optical Astronomy Observatories (NOAO), which is operated by the Association of Universities for Research in Astronomy, Inc., under contract to the National Science Foundation.

Table 2. Limiting magnitudes in the field of Q2302+029

	$m_{\text{obs}}$	$M_{\text{obs}}^a$	$k+EC\text{-corr}^b$	$M^c$	$M^{*d}$	$L/L^*$
<i>B</i>	25.2	-16.8	1.0	-17.8	-19.3	0.3
<i>R</i>	24.5	-17.4	0.6	-18.0	-20.2	0.1
<i>I</i>	22.8	-19.1	0.6	-19.7	-21.8	0.1
<i>J</i>	22.6	-19.3	0.4	-19.7	-22.7	0.06
<i>K</i>	21.1	-20.8	0.2	-21.0	-23.6	0.09

<sup>a</sup> observed absolute magnitudes assuming  $z = 0.7$ ,  $q_0 = 0.5$ ;

all values of  $M$  above assume  $h = 1$

<sup>b</sup>  $k+EC$ -corrections for  $z = 0.7$ —see text

<sup>c</sup>  $k+EC$ -corrected absolute magnitudes

<sup>d</sup>  $M^*$  from: *B*—Marzke et al. (1998); *I*—Metcalf et al. (1998);  
*R*—Lin et al. (1996); *J*—see text; *K*—Loveday (2000)

in Table 2. The limits are based on both a search for faint objects in the data frames, as well as a  $2\sigma$  limit calculated from the signal-to-noise of the sky in a circular aperture with a radius twice the seeing FWHM. These two estimates were found to agree closely, despite the obvious problem that the magnitudes of the faintest objects in a frame also have the largest errors. Due to the large area of the WFC CCDs, it was also possible to construct a histogram of the distribution of galaxy magnitudes in the optical and observe the magnitude at which the distribution begins to decline. This is a partial indicator of a magnitude limit, simply because the numbers of galaxies should continue to increase with increasing magnitude. Unfortunately, this estimate suffers from the fact that galaxy type, inclination, etc., also play a role in where the surface density of galaxies begins to decrease, so it does not offer a definitive measure of limiting magnitude. However, it does give an indication of the *completeness* in the image, and by plotting such histograms of galaxy magnitudes, we deduce that we are complete in *R* and *B* to about 0.5 mags brighter than the limits given in Table 2. In *I*, the distribution is less well peaked due to the smaller number of galaxies detected, and the completeness limit is about the same as the magnitude limit measured as described above.

### 2.3. Spectroscopic observations

Spectroscopic observations of objects in the field of Q2302+029 were obtained during the last run before de-commissioning of the Low Dispersion Survey Spectrograph-2 (LDSS-2) at the William Herschel Telescope (WHT) on La Palma, 1999-Aug-7, 9, & 10. A SITe1 2148x2148 CCD was used in conjunction

with the medium/red grating which gave a dispersion of  $\simeq 5.0 \text{ \AA pix}^{-1}$  and resolution of  $\simeq 12.0 \text{ \AA FWHM}$ .

We selected all objects with  $R = 15.0 - 23.0$  within the central 0.75 arcmins ( $\equiv 180 h^{-1} \text{ kpc}$  at  $z = 0.7$ ). To this we added objects with  $R = 20.0 - 22.0$  within an annulus of radius 0.75–4.0 arcmins. Our aim was to focus on objects closest to the QSO, while using the brighter sample to fill up slits in the outer parts of the field of view. In practice, because of the large number of objects in the catalog, and the limited amount of space on a mask for slits, the area was well sampled over the LDSS-2 field of view without any bias in location. Three LDSS-2 masks were employed, each covering a 5 arcmin radius field of view, and containing 21–27 1.5 arcsec wide and 10 arcsec long slits. We note that these did not include the full number of galaxies selected, and we are therefore incomplete to any magnitude limit. Total exposure times varied for each mask due to observing constraints: 6x, 4x, and 3x 1800 sec were recorded for the three masks. We were unable to observe any standard stars to provide flux calibration for the galaxies, but one radial velocity standard was observed to improve the accuracy of the redshift measurements.

The data were again reduced using IRAF, with each individual galaxy spectrum (and associated arc) ‘cut’ from the 2D frame. Although arcs were taken before each set of mask exposures, we noticed shifts in the wavelengths of sky lines from one exposure to the next within each exposure set. Hence an offset was applied to each spectrum to set the O I  $\lambda 6300.3$  sky line to its geocentric value. Redshifts were estimated manually, and refined by cross-correlation techniques when possible using the IRAF `fxcor` package.

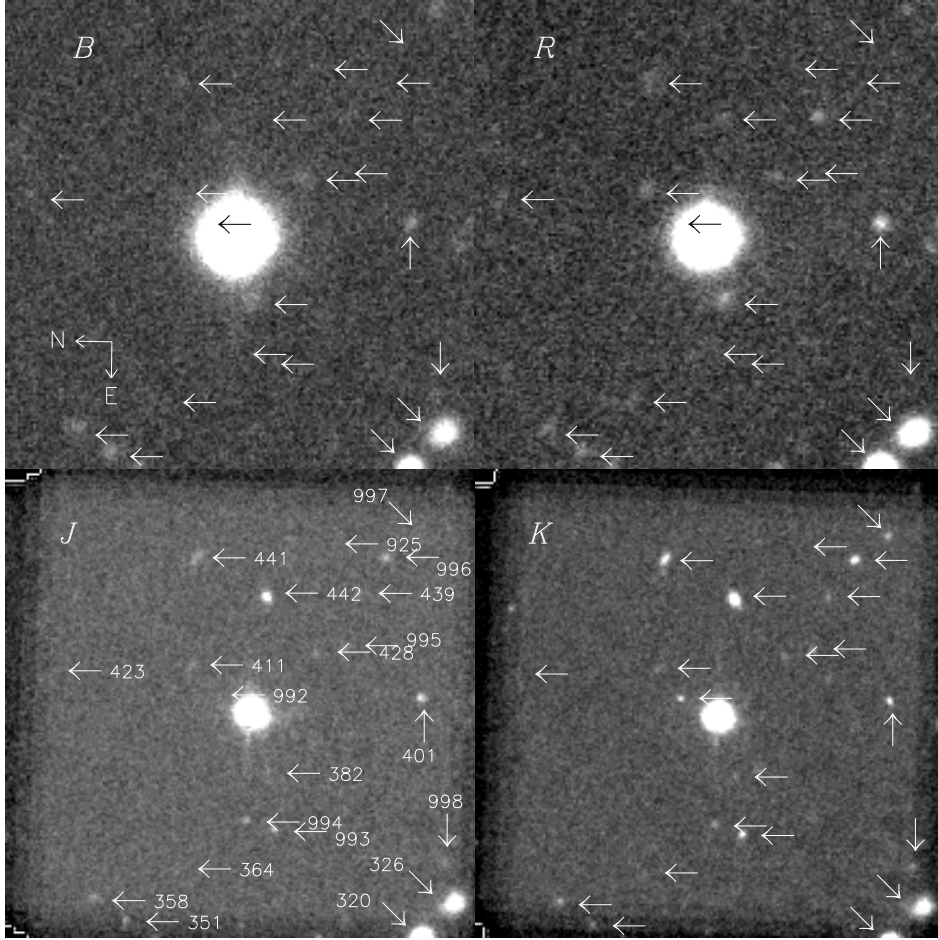


Fig. 2.— Portions of the *B*-, *R*-, *J*- and *K*-band images around Q2302+029, each 62x62 arcsec on a side (62 arcsec corresponds to  $247 h^{-1}$  kpc at  $z = 0.7$ ). The positions of all detected objects (even if detected in only a single band) are shown by arrows—for the sake of clarity, their numerical designations are only plotted on the *J*-band image. Although many detections are shown, most arise in the *K*-band, and probably represent galaxies at  $z > 1$ . Galaxy 401 is the only galaxy for which we have a spectroscopically confirmed redshift,  $z = 0.365$ .

### 3. Results

#### 3.1. Imaging

A montage of the inner 30 arcsecs around Q2302+029 in the *B*-, *R*-, *J*-, and *K*-band is shown in Figure 2. The most striking observation is that there are actually very few galaxies within this radius. The lack of detections in the *J*-band is the most telling, since these are our deepest images and are most sensitive to the old stellar populations at  $z = 0.7$ .

An obvious question is whether there could be a galaxy aligned precisely with the center of the QSO. We were unable to adequately remove the QSO Point Spread Functions (PSFs) from the optical images be-

cause the QSO profiles were saturated, and the resulting profile subtraction was poor. Instead, we concentrated on removing the unsaturated quasar profile from the *J*-band image, where we expect to be most sensitive to an intervening galaxy at  $z = 0.7$ , using the PSF of a standard star taken immediately prior to the observations of Q2302+029. The stellar PSF was scaled and shifted to produce a minimum  $\chi^2$  between it and the QSO profile, and the result was subtracted from the quasar image. We set the central 7x7 pixels to zero to allow a best fit to the profile wings alone, since this is where we are most likely to resolve a galaxy. The subtraction is presented in Figure 3. Some residuals are seen due to the finite signal-to-noise of the stan-

Table 3. Redshifts obtained in the field of Q2302+029

ID	Position (J2000.0)		$B$	$R$	$I$	$\theta$ ( $'$ )	$z$	$\rho$ ( $h^{-1}$ kpc)	$M_{\text{obs}}(R)$
	RA	DEC							
65	23:04:56.77	03:13:42.8	23.1	22.0	21.5	3.529	0.589	800.6	-19.5
91	23:04:55.15	03:10:55.5	22.0	20.7	20.4	2.678	0.3566	487.0	-19.6
117	23:04:54.70	03:12:59.5	22.7	21.6	21.5	2.719	0.590	617.2	-19.9
135	23:04:54.06	03:13:40.4	22.5	20.7	20.0	2.962	0.3165	504.0	-19.3
164	23:04:52.79	03:13:34.0	22.1	21.2	20.8	2.653	0.426	527.5	-19.5
251	23:04:49.49	03:12:05.2	22.7	21.9	21.0	1.172	0.7197	282.2	-20.0
265	23:04:48.55	03:11:25.5	23.1	20.2	19.0	0.958	0.5911	217.6	-21.3
291	23:04:48.32	03:12:42.7	22.8	21.5	21.2	1.259	0.5915	286.0	-20.0
325	23:04:47.21	03:09:25.8	24.2	21.8	20.8	2.406	0.327	417.1	-18.3
354	23:04:46.21	03:10:35.4	23.4	20.9	19.6	1.220	0.5915	277.1	-20.6
359	23:04:46.39	03:15:08.6	24.0	21.2	20.2	3.392	0.6453	792.4	-20.5
365	23:04:45.93	03:12:56.9	22.0	21.3	20.8	1.202	0.058	55.1	-14.9
368	23:04:45.67	03:12:24.4	23.5	21.4	20.6	0.660	0.59	149.4	-20.1
370	23:04:45.50	03:12:22.2	22.3	21.2	21.1	0.614	0.2565	91.9	-18.4
374	23:04:45.62	03:11:02.9	22.9	21.6	21.0	0.740	0.5880	167.8	-19.9
401 <sup>1</sup>	23:04:44.83	03:11:23.5	24.0	22.5	22.1	0.380	0.365	70.0	-17.9
417	23:04:44.29	03:12:55.6	22.9	21.7	21.5	1.169	0.4675	242.4	-19.2
480	23:04:42.51	03:10:16.9	21.1	20.4	20.2	1.610	0.4560	330.3	-20.5
488	23:04:41.56	03:13:36.2	20.9	19.1	18.2	2.021	0.3065	337.6	-20.9
492	23:04:42.47	03:10:19.2	>25.2	22.0	20.8	1.579	0.5910	358.6	-19.5
509	23:04:41.47	03:08:36.3	22.6	21.0	20.4	3.283	0.458	674.8	-19.9
548	23:04:40.76	03:09:29.3	23.0	22.0	21.0	2.512	0.6925	598.8	-19.9
593	23:04:38.92	03:11:52.8	22.1	20.8	20.2	1.514	0.0	...	...
748	23:04:31.99	03:11:18.7	21.6	20.3	19.4	3.272	0.2765	513.7	-19.4

<sup>1</sup> This is the only object with a determined redshift within the IRCAM field of view; we measure  $J = 20.8 \pm 0.2$  and  $K = 20.0 \pm 0.3$

dard star data, and do not represent the detection of an underlying galaxy. Although the signal-to-noise of the image is degraded from subtraction of an empirical PSF, we can still detect the majority of the faint galaxies cataloged from the unsubtracted frame, meaning that the magnitude limit is still  $J \sim 22.6$ . As Figure 3 shows, we detect nothing outside a radius of  $\sim 5$  pix from the center of the QSO, or 1.4 arcsec. This corresponds to  $6 h^{-1}$  kpc at  $z = 0.7$ .

### 3.2. Spectroscopy

We were able to measure 23 ‘secure’ redshifts in the field around Q2302+029 with LDSS-2. These are listed in Table 3, which gives the object ID, its position,  $R$ -,  $I$ -, and  $B$ -band magnitudes, separation,  $\theta$ , from the QSO sightline, derived redshift, corresponding separation,  $\rho$ , in  $h^{-1}$  kpc, and resulting absolute magnitude,  $M$ , without any  $k$ -correction applied (see

§4.1). The positions of these objects on the sky are shown overlaid on the  $R$ -band image in Figure 4. We note, without showing all the galaxy spectra obtained, that these represent only the redshifts we consider to be secure. For the majority of the galaxies observed, we were unable to deduce a redshift, largely because we had selected galaxies at magnitudes expected for intermediate-redshift, but which were close to the limit of the WHT’s sensitivity. The redshifts in Table 3 are quoted with varying degrees of precision; these crudely reflect the accuracy with which they are measured, which depends on the quality of the data.

We detect two galaxies at a redshift near that of the absorber, galaxy 548 at  $z \sim 0.6925$ , which is  $599 h^{-1}$  kpc away from the QSO sightline, and galaxy 251 at  $z = 0.7197$ , which is only  $282 h^{-1}$  kpc away. We discuss the likelihood that these are the absorbers in §4. In Figure 5 we plot a histogram of

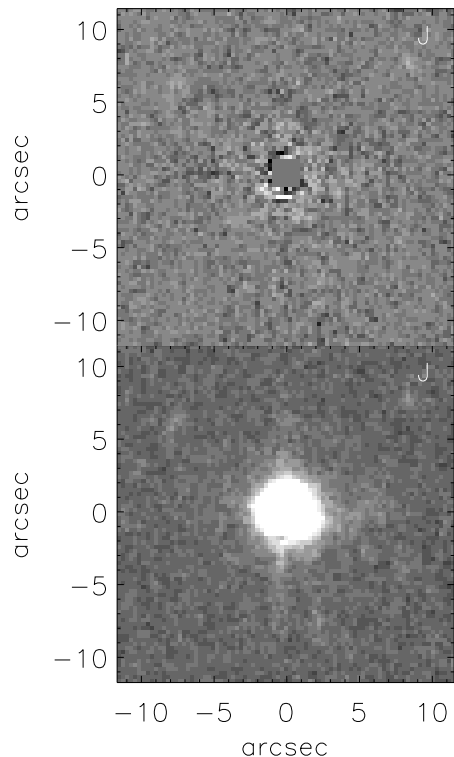


Fig. 3.— Results of our PSF subtraction in the  $J$ -band before (bottom) and after (top).

the redshift distribution for the 23 galaxies measured. Although the numbers are small, we detect an overdensity of galaxies at  $z \sim 0.59$ . We also discuss this apparent cluster of galaxies in §4.

We were able to obtain the redshift of one galaxy in IRCAM’s small field of view, that of galaxy 401 at  $z \approx 0.365$ . Although not at the redshift of the high ionization system, we note in passing that the galaxy is of interest in its own right; it lies  $70 h^{-1}$  kpc from the QSO sightline, and has a measured absolute magnitude of  $M_R = -18.2$  and  $M_B = -16.8$  (after applying a suitable  $k$ +EC-correction of 0.3 and 0.4 mags for  $R$  and  $B$  respectively, and assuming  $h = 1$ —see §4.1). An absorption line at  $1661.6 \text{ \AA}$  is identified by Jannuzi et al. (1998) as “C III  $\lambda 977$ ?” at  $z = 0.7016$ , although the difference between the measured and expected wavelength is large,  $-0.94 \text{ \AA}$ . We show the expected position of  $\text{Ly}\alpha$  at the redshift of galaxy 401 in Figure 8,

and although the error on the galaxy’s redshift is large, it is possible that the absorption line at  $1661.6 \text{ \AA}$  is  $\text{Ly}\alpha$  at  $z = 0.3667$ . The strength of the line and the galaxy’s luminosity are just about consistent with the relationships of sightline separation, luminosity, column density, and equivalent width found by Chen et al. (1998) for  $\text{Ly}\alpha$  absorbing galaxies, even though the line is strong (rest equivalent width  $W_\lambda = 1.28 \pm 0.12 \text{ \AA}$  for  $z = 0.3667$ ) and the galaxy faint, with a magnitude close to that of the Small Magellanic Cloud.

### 3.3. Photometric redshifts

Due to the difficulty in obtaining a significant number of galaxy redshifts at  $z = 0.7$  with a 4 m telescope, we developed algorithms to constrain a galaxy’s redshift photometrically. We used the synthetic stellar population models developed by Jimenez et al. (2000) which are determined by the spin,  $\lambda$ , of the dark halo of the galaxy, to produce galaxy SEDs. Heavens & Jimenez (1999) obtained closed analytic expressions for the SFR and gas fraction of a galaxy and full details can be found therein; to generalize, a value of  $\lambda = 0.02$  yields a SFR typical of an Sab galaxy, while  $\lambda = 0.10$  gives the SFR of an irregular galaxy.

In order to compute the photometric redshift of an observed galaxy we allowed our model parameters—age, redshift, star formation efficiency—to take any possible value and used a  $\chi^2$  minimization to find the best fitting values. Our approach is similar to that developed in Arnouts et al. (1999) but is contrary to that of other groups [e.g. Csabai et al. (1999); Driver et al. (1998)] who derive redshift templates from observations and/or a mixture of observations and models. Since the purpose of this paper is not to derive precise redshifts for every galaxy in the field of Q2302+029, which would be difficult considering the small number of photometric bands used, we will not enter into a detailed comparison of our fitting procedure with other redshifts surveys. We note, however, that we have made such comparisons, and that we were able to recover measured redshifts (such as those in the Hubble Deep Field) to an accuracy in redshift of  $\Delta z \sim 0.1$ .

As described in §1, these algorithms work best when a galaxy is observed in the infra-red, when the flux is observed at wavelengths beyond the peak of its SED. Below, therefore, we discuss the five brightest galaxies seen close to the QSO (that is, within the IRCAM field of view) that have no measured redshift and discuss the possibility that they could be at a  $z \sim 0.7$ .

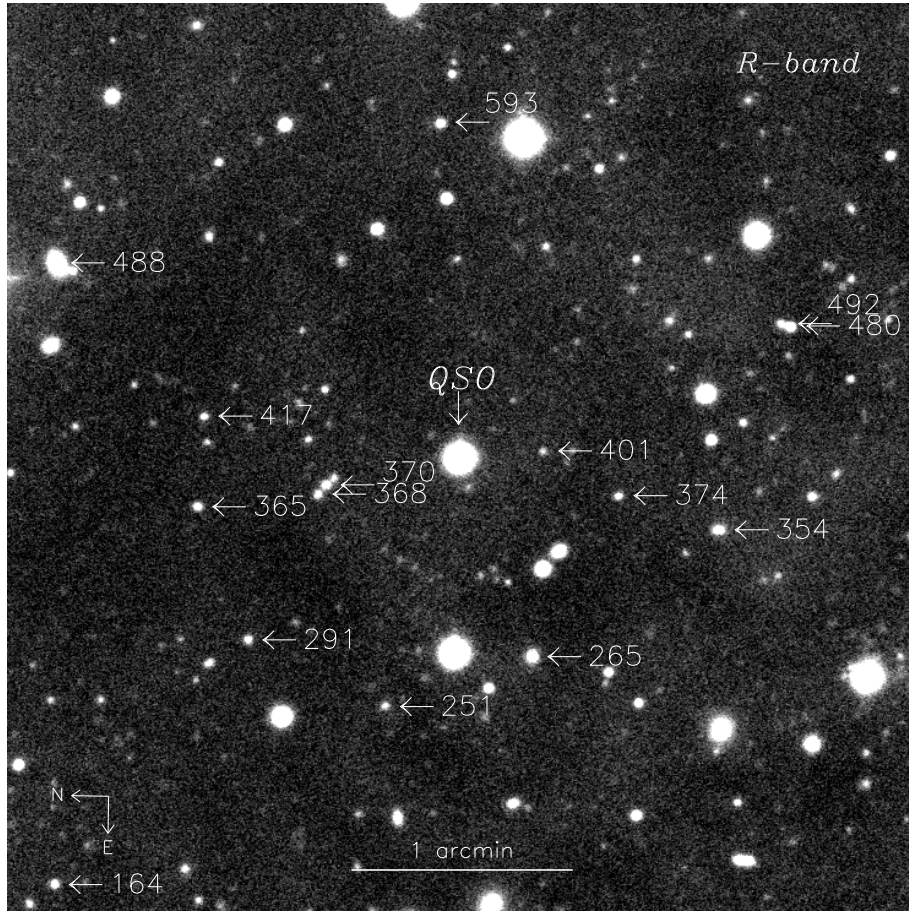


Fig. 4.— 4x4 arcmin section of the *R*-band image of Q2302+029 showing galaxies with spectroscopic redshifts. Object designations correspond to those given in Table 1 and Table 3.

First we note a general principle. In Figure 1 we plot the SED for a typical galaxy at  $z = 0$  and the same (younger) galaxy at  $z = 0.7$ . We also overplot the relative flux limits obtained from our images (diamonds) arbitrarily normalized such that  $F_\lambda(I)$  is close to the peak of the SED of the galaxy at  $z = 0.7$ . The figure shows that it is extremely difficult for any galaxy we detect in all four bands to be at a redshift of 0.7, essentially because the blue flux from the galaxy is predicted to be low. Only if the galaxy has a particularly high SFR can the blue flux be detected in the *B*-band from a galaxy at intermediate redshift.

326 — The derived photometric redshift is  $z_{\text{phot}} \sim 0.05$ . The optical images suggest that the galaxy is elliptical, while in the IRCAM images it appears more irregular. Archival HST WFPC2 images of the galaxy clearly reveal some spiral structure, although the over-

all morphology appears irregular. The galaxy is detected in all bands; Figure 6 shows that the photometric redshift is ill defined since the continuum is quite flat, and suggests that it might be possible for the galaxy to be at  $z = 0.7$  if very young. However, the unambiguous resolution of structure in the WFPC2 image clearly demonstrates that the galaxy must be at a fairly low redshift and cannot be at  $z \sim 0.7$ . The galaxy would also be unusually bright: applying suitable *k*- and EC-corrections (see §4.1) would give absolute magnitudes of  $M_R = -22.5$  and  $M_B = -21.3$ .

320 — *sextractor* defines the object to be a star in both optical and IR images. This is confirmed in the WFPC2 image.

441 & 442 — As shown in Figure 6 the relative distribution of the photometric points for both galaxies are completely incompatible with any galaxy at  $z \sim$



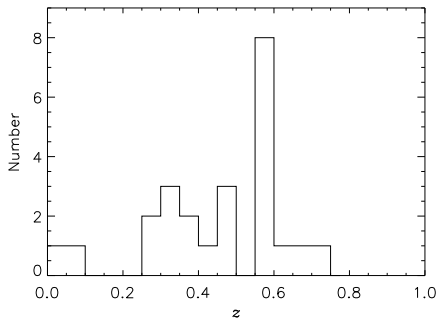


Fig. 5.— Redshift distribution of all the galaxies observed by LDSS-2 for which ‘secure’ redshifts could be obtained, i.e. those listed in Table 3. A peak at  $z = 0.59$  is clear.

0.7. Both must lie at  $z > 1$ , and to further demonstrate this, we include best-fit SEDs to the data points: for galaxy 441,  $z_{\text{phot}} \sim 1.9$ , while for 442  $z_{\text{phot}} \sim 2.0$ .

382 — This galaxy is just detected in  $R$  and so is included in our catalog, but it is not detected by *sextractor* in the remaining bands. In part, this is due to a combination of its faintness combined with its proximity to the QSO, where the background is higher, and in fact a visual inspection of the frames suggest that the galaxy might just be detected in  $B$ ,  $J$  &  $K$ . Although we cannot calculate a photometric redshift from only one color, we think it unlikely that the object could be at  $z = 0.7$ : the galaxy would have to be very young ( $\leq 2$  Gyr old), bright, with  $M_R = -19.9$ , and have an extremely high star formation rate to explain the detection in the  $B$ -band. Although these constraints are not impossible to satisfy in principle, they would be unusual, and with no reliable photometry, we can make no claim as to the galaxy being responsible for the high ionization system.

## 4. Discussion

### 4.1. The $z = 0.7$ high-ionization absorption system

We have been unable to detect any obvious bright galaxies within 30 arcsec of Q2302+029 which could be responsible for the  $z = 0.7$  high-ionization absorption system detected by Jannuzi et al. (1996). Our magnitude limits are given in Table 2; to estimate the absolute magnitudes that these observed limits correspond to, we have calculated the cosmological dimming,  $M_{\text{obs}}$ , then applied both a  $k$ - and Evolutionary-

correction (EC) to derive the absolute limiting magnitude,  $M$ , in individual bands. Besides having to correct a galaxy’s magnitude in a particular band for its redshifted SED (the standard  $k$ -correction), the galaxies observed at  $z \sim 0.7$  are younger than they would be now. So to compare galaxy magnitudes with those in the nearby universe, an EC-correction is also required. We have used our SED models discussed in §3.3 to estimate a combined  $k$ - and EC-correction; we have taken three values for the spin parameter of the halo ( $\lambda = 0.01, 0.05$  and  $0.1$ ) which represent all possible star formation histories in our models—from ellipticals to irregular types of galaxies. We have then formed each of the types at  $z > 2$  and computed the difference for each band between its  $z = 0$  value and the redshift of interest, resulting in the desired  $k$ +EC-correction. The correction obviously depends on the redshift of formation of the galaxy and its SFR. We find that for the IR bands the SFR and formation redshift are irrelevant since they sample mostly the old population, while in the optical the  $B$ -band  $k$ +EC corrections vary the most for different galaxy types: the maximum spread in the correction is  $\sim 0.5$  mags in the  $B$ -band, compared to only  $\sim 0.1$  in the  $K$ -band.

Table 2 also lists present day values of  $M^*$  [corresponding to the  $L^*$  break in the luminosity function (Schechter 1976)] for each band, taken from various galaxy surveys. We have been unable to find a value of  $M^*(J)$  in the literature, so we have used the value of  $M^*(K)$  given by Loveday (2000) and assumed  $J-K = 0.8$ . The final column gives the resulting value of  $L/L^*$ . In the optical we are able to find galaxies down to luminosities of  $\sim 1/10L^*$ , while in the  $J$ -band we are sensitive to galaxies with  $L \sim 1/20L^*$  or greater.

In our spectroscopic survey around the QSO, we detect two galaxies at a redshift near that of the absorber, galaxy 548 at  $z \sim 0.6925$ , which is  $599 h^{-1}$  kpc away from the QSO line of sight, and galaxy 251 at  $z = 0.7197$  which is only  $282 h^{-1}$  kpc away. Whether the detection of these two galaxies in our survey marks the existence of a cluster at  $z = 0.7$  is unclear. At this redshift, the sensitivity of our survey (as a function of magnitude limit and volume sampled) is falling rapidly, and the detection of two galaxies at  $z = 0.7$  might correspond to an ‘over-density’ of galaxies. Unfortunately, our survey was not designed to be complete to any specified magnitude limit, and we cannot calculate the sensitivity function of the survey to estimate whether the detection of two galaxies at the limit

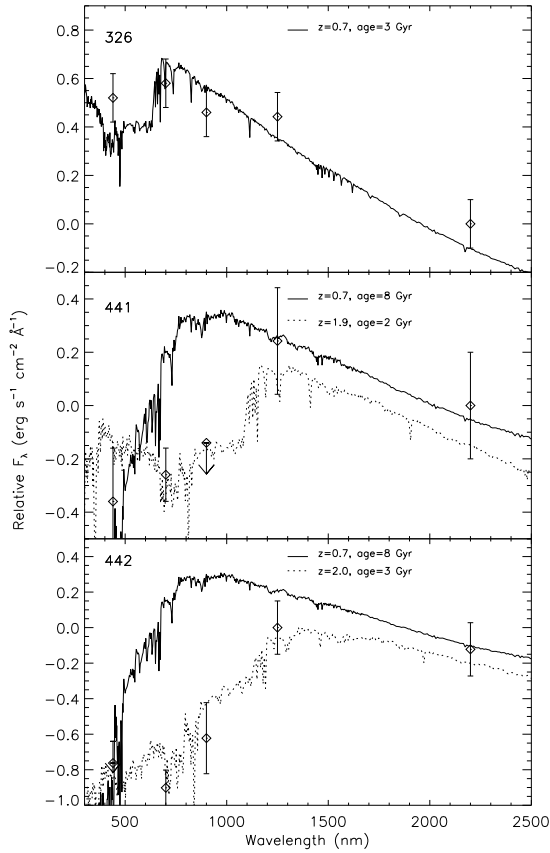


Fig. 6.— Comparison of theoretical SEDs to the photometry of the four brightest galaxies in IRCAM field of view. In all cases, we have constrained the SED to be at a redshift of 0.7 and varied the galaxy’s age, metallicity and SFR to best fit the data points (solid line).

of detectability is significant.

The difference in redshift between galaxy 251 and the narrow O VI system at  $z = 0.7106$  is  $\approx 1600 \text{ km s}^{-1}$ . The error in the redshift measurement is of order  $100\text{--}200 \text{ km s}^{-1}$ , so the velocity difference between galaxy and absorber is large, probably ruling out the galaxy as being associated with the absorber. The separation is also large compared to those found for Ly $\alpha$ -absorbing galaxies. If the O VI cross-section of a galaxy was larger than that found by Chen et al. (1998) for a Ly $\alpha$  halo, i.e.,  $> 160 h^{-1} \text{ kpc}$ , then the ionization at the edge of the halo would have to be sufficiently extreme to ionize the H I and produce O VI. In principle, the background UV radiation field can in-

duce O VI ions in sufficient number to produce the types of column densities detected, but the gas density must be low (i.e., the ionization parameter—the ratio of ionizing photons to total ionized+non-ionized hydrogen atoms—must be high) and/or the metallicity of the gas must be high (see, e.g., the discussion by Tripp & Savage 2000). This means that the path length must be extremely long, of order several hundred kpc. To obtain such a path length at the edge of a halo would require the radius to be  $\gg 200 h^{-1} \text{ kpc}$ , at which point the distinction between halo and the general IGM is severely blurred. Hence it seems unlikely that galaxy 251 is directly responsible for the absorption.

The remaining mechanisms which might be responsible for the high-ionization system towards Q2302+029 have been discussed by Jannuzi et al. (1996). To summarize, the absorption might arise from gas associated with: a) supernova ejecta in a galaxy along the line of sight, b) high velocity material ejected from the QSO, or c) intracluster material. Our observations suggest that there is unlikely to be a galaxy close to the line of sight in which a supernova occurred, although in principle the host could be perfectly aligned with the QSO image and not detected even with our subtraction of the QSO PSF in the *J*-band. Since the strength and breadth of absorption from supernovae ejecta decreases with time, this explanation can be easily rejected by re-observing the high ionization system and confirming that the system still exists.

The lack of any bright galaxy close to the sight-line actually supports both remaining hypotheses. In general, narrow absorption line systems have been considered unrelated to the QSO and its environs if  $\Delta v > 5000 \text{ km s}^{-1}$ ; even though the existence of an absorption system  $\sim 56,000 \text{ km s}^{-1}$  from the emission redshift of the QSO challenges our conventional view of the origin of metal-line absorption systems, the absence of any galaxies close to the line of sight is an obvious corollary. There is also some precedent for such an explanation in recent work by Hamann et al. (1997), which details the variability of both broad and narrow C IV and Si IV lines towards another QSO Q2343+125. In this case, the velocity difference between QSO and absorbing gas is  $\approx 24,000 \text{ km s}^{-1}$ , and the variability is the strongest evidence that the system is actually intrinsic to the QSO. Clearly, searching for variability in the absorption lines towards Q2302+029 will be a powerful test of whether the  $z = 0.7$  sys-

tem is intrinsic. Such data may soon be available (Januzzi et al., in preparation).

The third possibility suggested above, that we are seeing absorption by intracluster gas, is also problematic. If the absorption is due to the warm/hot gas which occurs in shocked regions collapsing with the dark matter, as suggested by the models, then the width of the absorption represents a cosmological distance, rather than an intrinsic velocity dispersion from thermal or turbulent motions. Thus, if the width of the structure is  $\sim 4000 \text{ km s}^{-1}$  wide, then the corresponding cosmological distance would be  $\sim 40 h^{-1} \text{ Mpc}$  (comoving). This would imply a rather special geometry, with the sightline passing *along* a filament—a rare, but not impossible alignment. If true though, would we not expect to see a high surface density of galaxies, due to the alignment? The hydrodynamical simulations which exist at present do not have sufficient resolution to estimate the number of galaxies along a shock front, but we can crudely estimate the surface density of galaxies we would expect to see in our IRCAM field of view. If we assume that the luminosity function (LF),  $\phi$ , of galaxies at  $z = 0.7$  is the same as the Schechter LF of the local universe, then we can simply integrate the LF

$$d\phi = 0.92 \phi^* (L/L^*)^{\alpha+1} \exp(-L/L^*) dM \quad (1)$$

between the observed magnitude limits and arbitrarily bright magnitudes. Here,  $\phi^*$  is the number of galaxies with luminosity  $L^*$  and  $\alpha$  parameterizes the shape of the function at magnitudes fainter than  $L^*$ . For the  $K$ -band, Loveday (2000) derives values of  $\alpha = -1.16$ ,  $M^*(K) = -23.6$ , and  $\phi^* = 0.012 h^3 \text{ Mpc}^{-3}$ . Integrating equation 1 using a minimum magnitude of  $M(K) = -21.0$  gives a total of  $\sim 0.03 h^3 \text{ Mpc}^{-3}$ . Similar values are derived for the  $J$ -band. This would imply that the surface density of galaxies in the  $40 h^{-1} \text{ Mpc}$  filament would be  $\sim 1 h^2 \text{ galaxy Mpc}^{-2}$ . Yet the field of view studied with IRCAM is only  $\sim 0.06 h^{-2} \text{ Mpc}^2$ —hence we clearly expect  $\ll 1$  galaxy over such a small field of view, consistent with our observations. Unsurprisingly, our pencil-beam along the sightline is simply too narrow to detect significant over-densities of galaxies. It thus remains possible that the sightline to Q2302+029 passes through a warm/hot gas filament along its length.

Finally, with regard to our search for O VI systems in general, we cannot say whether our results

towards Q2302+029 are indicative of the population of the O VI system as a whole. The absorption towards Q2302+029 is clearly pathological, since none of the other (apparently) intervening  $z < 1$  O VI systems detected so far are accompanied by the broad, high-ionization absorption systems seen towards Q2302+029. Only further imaging and spectroscopy of fields around QSOs showing  $z < 1$  O VI systems will reveal whether individual galaxies are responsible for O VI systems, as well as searches for O VI absorption in the spectra of background QSOs located near foreground galaxies.

#### 4.2. The cluster at $z \sim 0.59$ and associated absorption lines

Although we detect few galaxies close to the QSO sightline, our spectroscopic survey shows that we have detected a cluster of galaxies at  $z \sim 0.59$ . In Figure 7 we reproduce a portion of the G190H FOS spectrum published by Januzzi et al. (1996) and plot the positions of  $\text{Ly}\alpha$  absorption expected at the redshift of each galaxy, along with its separation from the QSO line of sight (in  $h^{-1} \text{ kpc}$ ).  $\text{Ly}\alpha$  is detected at  $z = 0.5904$ , and is strong: Januzzi et al. (1998) measure a rest equivalent width of  $1.25 \text{ \AA}$ , but suggest that there may be contamination by  $\text{Ly}\delta$  from a system at  $z = 1.0361$ . This higher- $z$  system is detected in  $\text{Ly}\alpha$ ,  $\text{Ly}\beta$ ,  $\text{Ly}\gamma$  and  $\text{Ly}\epsilon$ , making it relatively easy to calculate the expected equivalent width of  $\text{Ly}\delta$ . A simple curve of growth analysis is well able to reproduce the Lyman equivalent widths (to within the quoted errors) with  $\log(N) \simeq 15.6$  and  $b \simeq 55 \text{ km s}^{-1}$ , meaning that we expect  $W_\lambda(\text{Ly}\delta) \simeq 0.3 \text{ \AA}$ . Simply subtracting this from the total equivalent width of the  $z = 0.5904$   $\text{Ly}\alpha$  line leaves  $W_\lambda(\text{Ly}\alpha) \sim 1.0 \text{ \AA}$ . This is a relatively strong  $\text{Ly}\alpha$  line, and if the correlation of  $\text{Ly}\alpha$  equivalent width and galaxy separation found by Chen et al. (1998) for  $\text{Ly}\alpha$ -absorbing galaxies were to hold here, we would expect to find at least one galaxy at a separation of  $\approx 30 - 100 h^{-1} \text{ kpc}$ , and  $L/L^* > 0.3$ , i.e. well within our detection limits. We tentatively detect one galaxy at a separation of  $149 h^{-1} \text{ kpc}$  at  $z = 0.59$  (Table 3) which could in principle be responsible for the absorption. However, given the galaxy's separation, the line probably has too large an equivalent width to well fit the correlation found by Chen et al. (1998).

Ortiz-Gil et al. (1999) provide an example of  $\text{Ly}\alpha$  absorption associated with a group of galaxies towards Q1545+2101, where absorption may occur not from intragroup gas but from the overlapping halos of

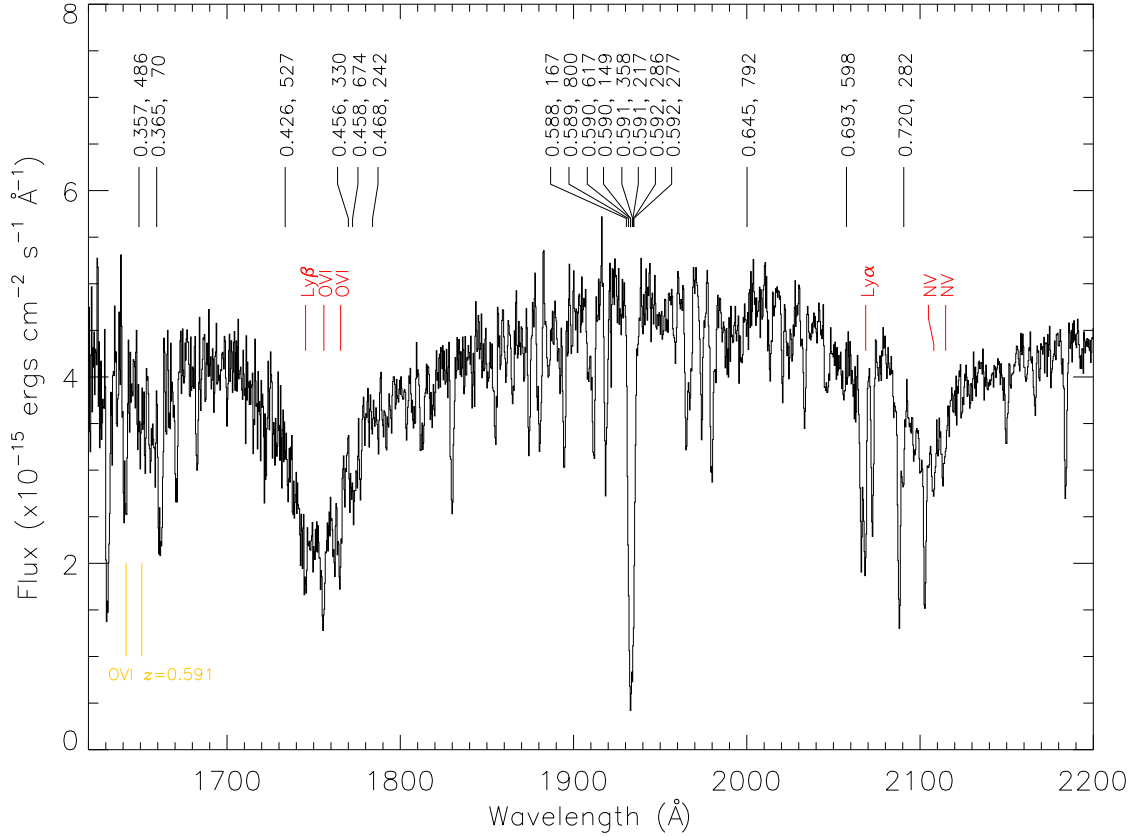


Fig. 7.— FOS spectrum of Q2302+029 (see Jannuzi et al. 1996). The positions of the narrow  $\text{Ly}\alpha$ ,  $\text{Ly}\beta$ , O VI and N V lines at  $z = 0.7106$  are shown just above the spectrum, superimposed on the broader lines discussed in the text. Above these, the wavelengths predicted for  $\text{Ly}\alpha$  from the galaxies in Table 3 are plotted, along with their redshift and their separation from the line of sight in  $h^{-1}$  kpc. The  $\text{Ly}\alpha$  absorption at the cluster redshift is clear. Below the spectrum, we also plot the expected position of O VI from the cluster at  $z = 0.59$ . This is shown more fully in Figure 8

individual galaxies comprising that group. Towards Q2302+029, it would seem that we have an example where strong absorption is clearly associated with a cluster of galaxies, but *not* with the halos of individual galaxies within that cluster. The comparison with Q1545+2101 is particularly interesting. The galaxies associated with the absorption towards Q1545+2101 range in absolute magnitude from  $M_R - 5\log h = -19.0$  to  $-20.8$ . As shown in Table 2, we would easily be able to detect these galaxies in  $R$  (and in the IR), so our inability to detect absorbing galaxies towards Q2302+029 is not because of insufficient sensitiv-

ity.<sup>3</sup> The most important piece of evidence linking the  $\text{Ly}\alpha$  absorption towards Q1545+2101 and the galaxies near the QSO sightline is the multicomponent structure of the  $\text{Ly}\alpha$  line. Ortiz-Gil et al. found eight individual  $\text{Ly}\alpha$  components spanning a total range of  $535 \text{ km s}^{-1}$ . It would be interesting to see if the  $\text{Ly}\alpha$  line arising at the same redshift as the cluster towards Q2302+029 also shows multicomponent structure at high resolution; clearly, smoother intragroup gas might not have the same complex structure as that seen towards Q1545+2101. We note, however, that the system towards Q1545+2101 may not be a good exam-

<sup>3</sup>A difference in redshift of 0.1, from  $z = 0.7$  in Table 2, to  $z = 0.59$  for the cluster, results in an *increase* in sensitivity by 0.4 mags

ple of absorption from a group of intervening galaxies, since the redshifts of the galaxies are the same as the QSO, i.e. this is an intrinsic system. The origin of the absorption systems in these systems is far from established, and the observed Ly $\alpha$  line may have nothing to do with galaxy halos.

The absorbing gas at  $z = 0.59$  is also a high-ionization system. In Figure 8 we reproduce a detail of the FOS spectrum around the area where O VI and Ly $\beta$  are expected, and show that the detections appear secure. There is unfortunately no corresponding O VI  $\lambda 1037$  line to confirm the identification, although this is plausibly lost in the noise. We note that there is no detection of N V at this redshift, even though the continuum is sufficiently clear to show any moderately strong lines, but Jannuzi et al. (1998) do list the detection of Si III  $\lambda 1206$ , Si IV  $\lambda 1393$ , and both C IV lines. Hence it appears that we have a second example of O VI absorption without any obvious nearby galaxies, at least within the  $\sim 160 h^{-1}$  kpc radius found by Chen et al. (1998) for Ly $\alpha$ -absorbing galaxies, unless the galaxy  $149 h^{-1}$  kpc away contributes to the absorption. Only a more complete search towards other sight-lines will reveal whether high-ionization systems are associated with galaxies at such large distances.

Again, it is possible that a cluster galaxy sits exactly on top of the QSO, and cannot be seen in our subtraction of the QSO profile. If so, we would now require that there exist *two* galaxies hidden from view (including the  $z \sim 0.7$  O VI absorber). This may be stretching the plausibility of this caveat. Absorption could also occur in a cluster galaxy fainter than our detection limits—this is a problem which has plagued the search for absorbing galaxies at all redshifts beyond  $z = 0$ , and our analysis is no different in being unable to address the problem beyond establishing secure magnitude limits in multiple photometric bands. Obviously, deeper images and more detailed spectroscopy should be possible with larger aperture telescopes. If we really are seeing intracluster gas not associated with any individual galaxy at  $z = 0.59$ , then higher resolution observations, allowing calculation of accurate column densities, may be useful in determining the physical conditions in the gas, which can in turn be compared with the predictions from the numerical simulations of the evolution of the warm/hot gas component.

We'd like to thank the many support astronomers who have helped us at all the telescopes used to obtain the data, and the WHT TAC who awarded us a substan-

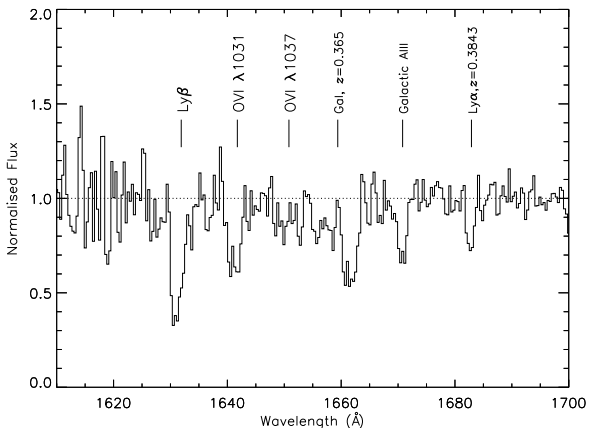


Fig. 8.— Detail of the FOS spectrum shown in the previous figure, centered at the expected position of O VI at the cluster's redshift of  $z = 0.59$ . In this case, the spectrum has been normalized. Ly $\beta$  is clearly detected, and a line probably corresponding to the O VI  $\lambda 1031$  line is clearly visible. We also label the expected wavelength of Ly $\alpha$  from the one galaxy in the IRCAM field of view whose redshift we were able to measure. This galaxy, 401, at  $z \approx 0.365$  is  $70 h^{-1}$  kpc from the line of sight, and is discussed in Section 3.2

tial allocation of LDSS-2 time. Thanks also to Todd Tripp for helpful discussions. Support for this work was provided in part through grants GO-06707.01 and GO-08165.01 from the Space Telescope Science Institute, which is operated by the Association of Universities for Research in Astronomy, Inc., under NASA contract NAS5-26555.

## REFERENCES

- Arnouts, S., Cristiani, S., Moscardini, L., Matarrese, S., Lucchin, F., Fontana, A., & Giallongo, E. 1999, *MNRAS*, 310, 540
- Bergeron, J. 1986, *A&A*, 155, L8
- Bergeron, J. & Boisse, P. 1991, *A&A*, 243, 344
- Bergeron, J., Petitjean, P., Sargent, W. L. W., Bahcall, J. N., Boksenberg, A., Hartig, G. F., Jannuzi, B. T., Kirhakos, S., Savage, B. D., Schneider, D. P., Turnshek, D. A., Weymann, R. J., & Wolfe, A. M. 1994, *ApJ*, 436, 33
- Bertin, E. & Arnouts, S. 1996, *A&AS*, 117, 393
- Bowen, D. V., Blades, J. C., & Pettini, M. 1996, *ApJ*, 464, 141
- Bowen, D. V., Pettini, M., & Boyle, B. J. 1998, *MNRAS*, 297, 239
- Burles, S. & Tytler, D. 1996, *ApJ*, 460, 584
- Cen, R. & Ostriker, J. P. 1999, *ApJ*, 514, 1
- Chen, H. W., Lanzetta, K. M., Webb, J. K., & Barcons, X. 1998, *ApJ*, 498, 77
- Csabai, I., Connolly, A., Szalay, A., & Budavari, T. 1999, *astro-ph*, 9910389
- Driver, S. P., Fernandez-Soto, A., Couch, W. J., Odewahn, S. C., Windhorst, R. A., Phillips, S., Lanzetta, K., & Yahil, A. 1998, *ApJL*, 496, L93
- Hamann, F., Barlow, T. A., & Junkkarinen, V. 1997, *ApJ*, 478, 87
- Heavens, A. F. & Jimenez, R. 1999, *MNRAS*, 305, 770
- Jannuzi, B. T., Bahcall, J. N., Bergeron, J., Boksenberg, A., Hartig, G. F., Kirhakos, S., Sargent, W. L. W., Savage, B. D., Schneider, D. P., Turnshek, D. A., Weymann, R. J., & Wolfe, A. M. 1998, *ApJS*, 118, 1
- Jannuzi, B. T., Hartig, G. F., Kirhakos, S., Sargent, W. L. W., Turnshek, D. A., Weymann, R. J., Bahcall, J. N., Bergeron, J., Boksenberg, A., Savage, B. D., Schneider, D. P., & Wolfe, A. M. 1996, *ApJ*, 470, L11
- Jimenez, R., Dunlop, J., Padoan, P., and James MacDonald, J. P., & Jorgensen, U. 2000, *MNRAS*, in press
- Lanzetta, K. M., Bowen, D. B., Tytler, D., & Webb, J. K. 1995, *ApJ*, 442, 538
- Lanzetta, K. M., Wolfe, A. M., Altan, H., Barcons, X., Chen, H. W., Fernandez-Soto, A., Meyer, D. M., Ortiz-Gil, A., Savaglio, S., Webb, J. K., & Yahata, N. 1997, *AJ*, 114, 1337
- Le Brun, V., Bergeron, J., & Boisse, P. 1996, *A&A*, 306, 691
- Le Brun, V., Bergeron, J., Boisse, P., & Deharveng, J. M. 1997, *A&A*, 321, 733
- Lin, H., Kirshner, R. P., Shectman, S. A., Landy, S. D., Oemler, A., Tucker, D. L., & Schechter, P. L. 1996, *ApJ*, 464, 60
- Loveday, J. 2000, *MNRAS*, 312, 557
- Lu, L. & Savage, B. D. 1993, *ApJ*, 403, 127
- Marzke, R. O., da Costa, L. N., Pellegrini, P. S., Willmer, C. N. A., & Geller, M. J. 1998, *ApJ*, 503, 617
- Metcalfe, N., Ratcliffe, A., Shanks, T., & Fong, R. 1998, *MNRAS*, 294, 147
- Morris, S. L., Weymann, R. J., Dressler, A., McCarthy, P. J., Smith, B. A., Terriale, R. J., Giovanelli, R., & Irwin, M. 1993, *ApJ*, 419, 524
- Ortiz-Gil, A., Lanzetta, K. M., Webb, J. K., Barcons, X., & Fernández-Soto, A. 1999, *ApJ*, 523, 72
- Rao, S. M. & Turnshek, D. A. 1998, *ApJ*, 500, L115
- Schechter, P. 1976, *ApJ*, 203, 297
- Shull, J. M., Stocke, J. T., & Penton, S. 1996, *AJ*, 111, 72
- Steidel, C. C., Dickinson, M., & Persson, S. E. 1994, *ApJ*, 437, L75
- Stocke, J. T., Shull, J. M., Penton, S., Donahue, M., & Carilli, C. 1995, *ApJ*, 451, 24
- Sutherland, R. S. & Dopita, M. A. 1993, *ApJS*, 88, 253
- Tripp, T. M., Lu, L., & Savage, B. D. 1998, *ApJ*, 508, 200

Tripp, T. M. & Savage, B. D. 2000, astro-ph, 0004135

Tripp, T. M., Savage, B. D., & Jenkins, E. B. 2000, ApJ, 534, L1

van Gorkom, J. H., Carilli, C. L., Stocke, J. T., Perlman, E. S., & Shull, J. M. 1996, AJ, 112, 1397

Table 1: Photometry of galaxies detected near the sightline of Q2302+029

ID	Position (J2000.0)		$B$	$R$	$I$	$J$	$K$	$\theta$
	RA	DEC						(arcmins)
320	23:04:46.96	03:11:23.1	20.9	18.4	17.0	16.0	15.1	0.628
326	23:04:46.64	03:11:18.8	21.6	20.0	19.5	18.5	17.4	0.618
330	23:04:47.21	03:11:32.5	>25.2	22.5	20.9	...	...	0.604
338	23:04:47.16	03:11:35.5	>25.2	23.1	>22.8	...	...	0.575
342	23:04:47.10	03:11:40.0	>25.2	22.5	22.9	...	...	0.542
345	23:04:46.98	03:11:36.5	>25.2	22.6	22.4	...	...	0.527
347	23:04:47.19	03:11:53.3	>25.2	24.0	>22.8	...	...	0.567
349	23:04:46.96	03:11:57.8	24.5	23.7	>22.8	...	...	0.533
350	23:04:47.12	03:11:50.9	25.7	24.6	>22.8	...	...	0.542
351	23:04:46.83	03:12:01.8	24.2	23.5	>22.8	>22.6	>21.1	0.532
357	23:04:44.97	03:11:46.2	15.8	15.5	15.2	14.7	13.8	0.000
358	23:04:46.65	03:12:06.3	24.0	23.9	>22.8	22.1	19.4	0.537
364	23:04:46.36	03:11:55.1	>25.2	24.3	>22.8	>22.6	>21.1	0.377
370	23:04:45.50	03:12:22.2	22.3	21.2	21.1	...	...	0.614
373	23:04:46.00	03:11:14.8	>25.2	24.0	>22.8	...	...	0.583
382	23:04:45.51	03:11:43.6	>25.2	22.6	>22.8	>22.6	>21.1	0.142
385	23:04:45.38	03:12:20.1	>25.2	22.1	20.9	...	...	0.574
396	23:04:45.03	03:11:17.0	24.4	23.4	>22.8	...	...	0.487
401	23:04:44.83	03:11:23.5	24.0	22.5	22.1	20.8	20.0	0.380
403	23:04:44.82	03:11:15.5	24.4	22.8	21.5	...	...	0.513
411	23:04:44.57	03:11:53.9	>25.2	23.4	>22.8	>22.6	>21.1	0.163
419	23:04:44.40	03:12:21.8	24.4	23.4	22.3	...	...	0.610
423	23:04:44.64	03:12:12.5	>25.2	24.5	>22.8	>22.6	>21.1	0.446
428	23:04:44.44	03:11:37.2	24.9	23.9	>22.8	22.6	>21.1	0.200
439	23:04:43.92	03:11:31.9	>25.2	23.1	>22.8	22.6	20.9	0.354
441	23:04:43.63	03:11:53.8	25.3	23.6	>22.8	20.5	18.9	0.358
442	23:04:43.93	03:11:44.2	>25.2	24.1	22.6	20.0	18.1	0.262
484	23:04:42.99	03:11:20.6	24.3	24.0	>22.8	...	...	0.653
493	23:04:42.80	03:11:40.2	>25.2	24.4	>22.8	...	...	0.551
494	23:04:42.72	03:11:42.6	24.8	24.2	>22.8	...	...	0.565
925	23:04:43.49	03:11:36.4	25.9	>24.5	>22.8	>22.6	>21.1	0.404
932	23:04:42.50	03:11:32.7	25.1	>24.5	>22.8	...	...	0.656
992	23:04:44.83	03:11:51.0	>25.2	>24.5	>22.8	>22.6	19.7	0.087
993	23:04:46.02	03:11:42.6	>25.2	>24.5	>22.8	22.0	19.8	0.269
994	23:04:45.94	03:11:46.2	>25.2	>24.5	>22.8	22.2	20.8	0.242
995	23:04:44.38	03:11:33.6	>25.2	>24.5	>22.8	21.8	20.9	0.256
996	23:04:43.60	03:11:28.4	>25.2	>24.5	>22.8	21.0	19.0	0.453
997	23:04:43.41	03:11:24.2	>25.2	>24.5	>22.8	>22.6	19.2	0.535
998	23:04:46.28	03:11:20.3	>25.2	>24.5	>22.8	>22.6	19.8	0.542
999	23:04:42.82	03:11:20.7	>25.2	>24.5	>22.8	...	...	0.685
1000	23:04:45.82	03:12:22.4	>25.2	>24.5	>22.8	...	...	0.640